J. Fluid Mech. (2019), *vol.* 867, *pp.* 949–968.
doi:10.1017/jfm.2019.169

Lubricating motion of a sphere towards a thin porous slab with Saffman slip condition

Sondes Khabthani[1], Antoine Sellier[2,†] and François Feuillebois[3]

[1]Laboratoire Ingénierie Mathématique, École Polytechnique de Tunisie, rue El Khawarezmi, BP 743, La Marsa, Tunisia

[2]LadHyX, École Polytechnique, 91128 Palaiseau CEDEX, France

[3]LIMSI-CNRS, UPR 3251, BP 133, 91403 Orsay CEDEX, France

(Received 7 December 2018; revised 17 February 2019; accepted 19 February 2019; first published online 28 March 2019)

Near-contact hydrodynamic interactions between a solid sphere and a plane porous slab are investigated in the framework of lubrication theory. The size of pores in the slab is small compared with the slab thickness so that the Darcy law holds there. The slab is thin: that is, its thickness is small compared with the sphere radius. The considered problem involves a sphere translating above the slab together with a permeation flow across the slab and a uniform pressure below. The pressure is continuous across both slab interfaces and the Saffman slip condition applies on its upper interface. An extended Reynolds-like equation is derived for the pressure in the gap between the sphere and the slab. This equation is solved numerically and the drag force on the sphere is calculated therefrom for a wide range of values of the slab interface slip length and of the permeability parameter $\beta = 24k^*R/(e\delta^2)$, where k^* is the permeability, e is the porous slab thickness, R is the sphere radius and δ is the gap. Moreover, asymptotics expansions for the pressure and drag are derived for high and low β. These expansions, which agree with the numerics, are also handy formulae for practical use. All results match with those of other authors in particular cases. The settling trajectory of a sphere towards a porous slab in a fluid at rest is calculated from these results and, as expected, the time for reaching the slab decays for increasing slab permeability and upper interface slip length.

Key words: lubrication theory, porous media

1. Introduction

Many applications in chemical engineering, water filtration and biology involve the motion of solid particles suspended in a Newtonian fluid near a porous slab or membrane. For instance, in filtration technology the problem of membrane clogging appears when particles approach very close to the membrane. This leads to membrane fouling (see for instance Le-Clech, Chen & Fane (2006) and references therein).

The filtration flow field of a viscous fluid near an isotropic porous slab is usually modelled using Navier–Stokes equations in the fluid and either Darcy (1856) or Brinkman (1947) equations in the porous medium. In the Darcy equation the isotropic

† Email address for correspondence: sellier@ladhyx.polytechnique.fr

porous medium is characterized by its (positive) permeability, denoted here as k^*. The size of pores is of order $\sqrt{k^*}$. The more complicated case of an anisotropic porous medium is modelled with a permeability matrix; see e.g. Karmakar & Raja Sekhar (2018).

The Brinkman equation being mathematically more general than the Darcy equation, the matching of the fluid and porous domains is simply done by prescribing continuity of the velocity and stress across the permeable interface. On the other hand, the use of the Darcy equation requires specific boundary conditions on the interface. Thus, there is a large body of literature devoted to this topic; see e.g. Nield & Bejan (2006). The conditions depend in general on the interface curvature. Henceforth, attention is restricted to a plane interface. The simplest boundary conditions are the continuity of normal velocity and pressure together with the no-slip condition for the tangential velocity. These conditions, which are physically valid at scales much larger than the size of pores, are widely employed. For instance Ramon *et al.* (2013), whose results will be compared to the present work, use such conditions. A more elaborate set of conditions valid at pore size was proposed by Saffman (1971). This allows a slip of the tangential velocity on the fluid side of the interface. As shown by Saffman (1971), this is the next approximation in an expansion for small $\sqrt{k^*}/a$, where a is a typical length scale in the fluid (for instance, the size of a particle embedded in the fluid). Note also that the Saffman slip condition is an extension of the Navier (1823) slip condition for an impermeable wall. The Navier condition involves a slip length. This model has been shown to be also relevant for rough walls (see Lecoq *et al.* (2004)). Even more general conditions were proposed either for the tangential velocity by Beavers & Joseph (1967) or for the shear stress by Ochoa-Tapia & Whitaker (1995*a*,*b*) and this is an ongoing research field. These more refined model conditions will not be considered here. Theoretically, the slip length of a linear shear flow along a porous wall is obtained by dividing the (tangent) slip velocity on the wall by the local shear rate. Practically, the needed shear flow profile near the porous wall is obtained by different experimental techniques. For instance, Carotenuto & Minale (2011) used measurement from a constant-stress rheometer to infer the velocity profile and Wu & Mirbod (2018) measured directly the velocity profile by particle image velocimetry. For anisotropic porous media the interface might also be anisotropic and another anisotropic Saffman-like slip condition would then apply, generalizing the case of an impermeable anisotropic plane slip wall (see Bazant & Vinagradova (2008)).

Consider now particles near a plane impermeable or permeable solid boundary. Assuming a dilute suspension of spheres, we are concerned with a single solid impermeable sphere located close to a plane surface on which one of the above boundary conditions applies.

The case of a sphere near an impermeable slip plane has been handled in several works. Starting with the axisymmetric problem of a slip sphere translating normal to an impermeable plane slip wall (using the Navier condition for both impermeable surfaces), Goren (1973), Hocking (1973) and Vinogradova (1995) considered the lubrication problem when the sphere is very close to the wall. Note that Goren (1973) and Vinogradova (1995) allow two different slip lengths on the sphere and on the wall, as opposed to Hocking (1973). Moreover, Goren (1973) implemented the bipolar coordinates technique to solve the problem of arbitrary sphere–wall gap for equal slip lengths. The asymmetric problem of a sphere translating and/or rotating parallel to a plane impermeable wall has been solved, using bipolar coordinates, by Davis, Kezirian & Brenner (1994) when there is slip either on the wall or on

the sphere. The asymmetric case of a slip sphere immersed in an ambient shear flow above a slip plane impermeable wall was also treated in Luo & Pozrikidis (2008) by resorting to a boundary element method. Finally, the asymmetric case of a no-slip sphere embedded in an ambient linear and quadratic shear flow parallel to a slip impermeable wall was solved by Loussaief, Pasol & Feuillebois (2015) and Ghalia, Feuillebois & Sellier (2016), respectively, using the bipolar coordinates technique.

The case of a no-slip impermeable sphere located near a plane permeable surface (for instance near a porous half-space or near a porous slab or membrane with finite thickness and parallel plane boundaries) has also been the subject of various articles. The axisymmetric problem of a sphere translating normal to a no-slip permeable plane has been solved, using bipolar coordinates for non-zero gap and tangent bipolar coordinates for the contact problem: for the case of a thin no-slip permeable membrane we may cite Goren (1979) for arbitrary sphere–plane gap and Nir (1981) for a sphere in contact. In a similar way, the problem of a sphere near a porous half-space was considered by Sherwood (1988) for the contact case and Michalopoulou, Burganos & Payatakes (1992) otherwise. The axisymmetric problem of a sphere translating towards the permeable and no-slip plane upper surface of a porous slab with finite thickness is more involved, since it also requires the modelling of the fluid flow inside the slab, by using either Darcy or Brinkman equations. For a sphere close to the slab, a lubrication analysis of the flow field in the thin liquid film is possible. Such an analysis can be derived from Lin, Lu & Yang (2001) for a no-slip boundary condition at the motionless lower slab surface and a Brinkman model inside the slab. Another lubrication analysis was performed by Ramon *et al.* (2013) who deal with a Darcy model in a thin slab with the no-slip boundary condition on its upper boundary and a prescribed uniform pressure on its lower boundary. The same flow field configuration, but for the more general case of a sphere at some distance of the slab, was solved by Debbech, Elasmi & Feuillebois (2010) using the method of fundamental solution. This solution is based on the calculation of the Green tensor for the Stokes flow near a Darcy porous slab by Elasmi & Feuillebois (2001). The more general case of a porous slab of arbitrary thickness with the same boundary condition (in particular no slip on the upper boundary and uniform pressure at the lower boundary) was solved later by Elasmi & Feuillebois (2003) using the boundary integral method.

For a small wall–particle gap (around of 5 % of the sphere radius), the boundary integral method suffers from some lack of accuracy. This is the incentive to propose here a lubrication analysis for the axisymmetric problem of a sphere translating normal and close to a thin porous slab. The Darcy equation applies in the thin slab and the Saffman slip condition is prescribed on its upper side.

The paper is organized as follows. The addressed filtration problem and adopted numerical method are presented in § 2. Asymptotic predictions for large and small normalized permeability and numerical results obtained for the pressure on the sphere and the resulting drag force are presented in § 3. The settling of the sphere is then examined in § 4 and finally conclusions are given in § 5.

2. Filtration problem and numerical procedure

This section presents the problem of the pressure distribution on a solid sphere translating towards a permeable slip porous slab and the solving numerical procedure.

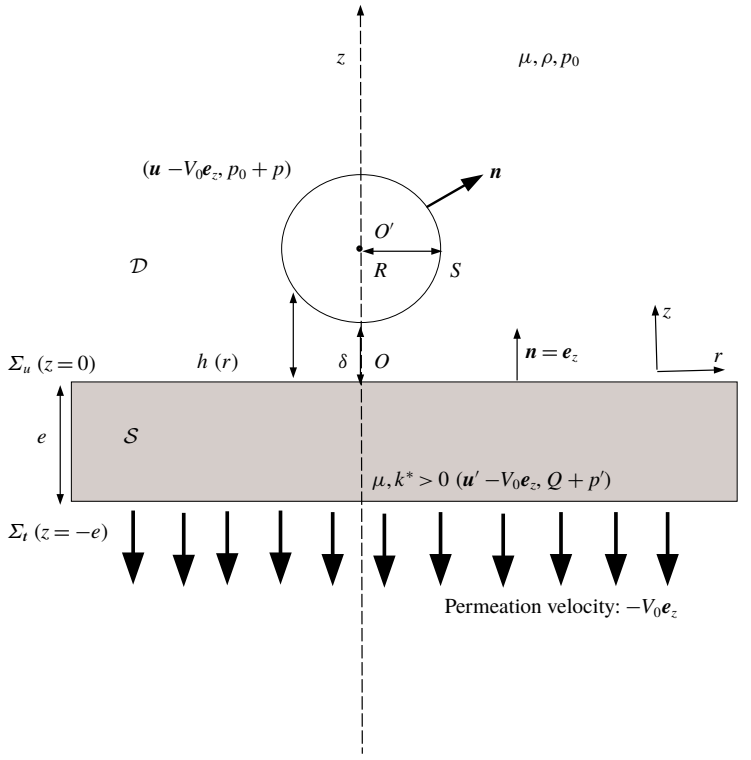

FIGURE 1. A solid sphere with radius R settling towards a permeable porous slab $\mathcal{S}$ with permeability $k^* > 0$ and thickness e.

2.1. *Considered axisymmetric flow fields*

Consider, as sketched in figure 1, a Newtonian fluid (liquid or gas), with uniform density ρ and viscosity μ, embedding a porous slab domain $\mathcal{S}$ with thickness $e > 0$ in $-e < z < 0$ and two open fluid domains in $z < -e$ and $z > 0$. In the absence of the sphere, the fluid velocity is uniform, i.e. $-V_0\boldsymbol{e}_z$ in each domain. The fluid pressure is a constant $p_0 > 0$ for $z > 0$, zero for $z < -e$ and obeys the Darcy equation in the slab with uniform Darcy permeability $k^* > 0$. The pressure Q in the slab therefore reads $Q = \mu V_0(z + e)/k^*$. Finally, the fluid pressure is continuous across the porous slab boundaries $z = -e$ and $z = 0$, called here the lower and upper surfaces Σ_l and Σ_u, respectively. Thus, the so-called background permeation velocity V_0 in the whole space, imposed by the pressure p_0, is given by $V_0 = p_0 k^*/(\mu e)$.

A solid sphere, with centre O' and radius R, is immersed above the slab in the ambient permeation flow $-V_0\boldsymbol{e}_z$. It translates towards the slab at the steady velocity $-V_p\boldsymbol{e}_z$. The resulting perturbed fluid flow has a quasi-steady velocity $\boldsymbol{u} - V_0\boldsymbol{e}_z$ and a pressure $p_0 + p$ in the fluid domain $\mathcal{D}$ above the slab and a quasi-steady velocity $\boldsymbol{u}' - V_0\boldsymbol{e}_z$ and a pressure $Q + p'$ in the slab $\mathcal{S}$. As will be shown below, it is irrelevant to consider in the present work the velocity and pressure disturbances occurring below the slab (i.e. in the $z < -e$ domain) and such quantities are thus henceforth discarded. The flow is governed by the quasi-steady Navier–Stokes and Darcy equations in $\mathcal{D}$ and $\mathcal{S}$, respectively. Accordingly,

$$\rho(\boldsymbol{u} - V_0\boldsymbol{e}_z)\cdot\boldsymbol{\nabla}\boldsymbol{u} = -\boldsymbol{\nabla}p + \mu\boldsymbol{\nabla}^2\boldsymbol{u} \quad \text{and} \quad \boldsymbol{\nabla}\cdot\boldsymbol{u} = 0 \quad \text{in } \mathcal{D}, \tag{2.1a,b}$$

$$\boldsymbol{u}' = -\frac{k^*}{\mu}\boldsymbol{\nabla} p' \quad \text{and} \quad \boldsymbol{\nabla}\cdot\boldsymbol{u}' = 0 \quad \text{in } \mathcal{S}. \tag{2.2a,b}$$

The problem (2.1)–(2.2) must be supplemented with proper boundary conditions. Denoting by S the sphere boundary, the following far-field condition and no-slip boundary condition on the sphere apply:

$$(\boldsymbol{u}, p) \to (\boldsymbol{0}, 0) \quad \text{at } \infty, \quad \boldsymbol{u} = (V_0 - V_p)\boldsymbol{e}_z \quad \text{on } S. \tag{2.3a,b}$$

Additional conditions on the permeable $z = 0$ upper surface Σ_u are also needed. The continuity of both the velocity component normal to the slab and the pressure holds there

$$\boldsymbol{u}\cdot\boldsymbol{e}_z = \boldsymbol{u}'\cdot\boldsymbol{e}_z, \quad p = p' \quad \text{on } \Sigma_u(z=0). \tag{2.4a,b}$$

In the present work we also impose on Σ_u the Saffman (1971) (SA) slip boundary condition for the velocities $\boldsymbol{u}_t = \boldsymbol{u} - (\boldsymbol{u}\cdot\boldsymbol{e}_z)\boldsymbol{e}_z$ tangent to the slab. This condition reads

$$\text{SA:} \frac{\partial \boldsymbol{u}_t}{\partial z} = \left(\frac{\sigma}{\sqrt{k^*}}\right)\boldsymbol{u}_t \quad \text{on } \Sigma_u(z=0), \tag{2.5}$$

where the dimensionless slip parameter σ is positive. In practice, the Darcy law is obtained when the porous slab thickness e is much larger than the typical length of the pores $r_p = \sqrt{k^*}$. Accordingly, we assume that $e \gg \sqrt{k^*}$. In addition, the Saffman condition suggests introducing the so-called slab slip length $l = \sqrt{k^*}/\sigma$ which means that $\sigma = r_p/l$. The widely employed Navier (1823) slip condition on a solid and impermeable wall with given slip length $l > 0$ is retrieved by taking $\sigma = \sqrt{k^*}/l$ and letting k^* vanish. The case of a permeable and no-slip slab, considered in Ramon *et al.* (2013), is retrieved from the Saffman boundary condition with $k^* > 0$ and $\sigma \to \infty$. In summary, the retained assumptions are

$$\sqrt{k^*} \ll e; \quad \sigma > 0. \tag{2.6a,b}$$

For symmetry reasons both flows $(\boldsymbol{u}, p)$ and $(\boldsymbol{u}', p')$ are axisymmetric, with no swirl, about the $(O, \boldsymbol{e}_z)$ axis. We use Cartesian coordinates (O, x, y, z) and cylindrical coordinates (r, z) with the unit local vector $\boldsymbol{e}_r$ such that $r = \{x^2 + y^2\}^{1/2}$ and $\boldsymbol{x} = z\boldsymbol{e}_z + r\boldsymbol{e}_r$. Accordingly, $p(\boldsymbol{x}) = p(r, z)$ and $\boldsymbol{u}(\boldsymbol{x}) = u_r(r, z)\boldsymbol{e}_r + w(r, z)\boldsymbol{e}_z$ with similar properties for p' and $\boldsymbol{u}'$, the cylindrical components of which are u_r' and w'. The stress tensor of the flow field $(\boldsymbol{u}, p)$ is denoted as $\boldsymbol{\sigma}$. For symmetry reasons, the force $\boldsymbol{F}_s$ experienced by the translating sphere then reads $\boldsymbol{F}_s = F_s\boldsymbol{e}_z$ with

$$F_s = \int_S \boldsymbol{e}_z\cdot[\boldsymbol{\sigma}\cdot\boldsymbol{n} - p_0\boldsymbol{n}]\,\mathrm{d}S = \int_S \boldsymbol{e}_z\cdot\boldsymbol{\sigma}\cdot\boldsymbol{n}\,\mathrm{d}S, \tag{2.7}$$

where $\boldsymbol{n}$ denotes the unit normal vector on S pointing into the liquid (see figure 1). The sphere centre is O' and each point M on its boundary S is specified by an angle $\theta \in [0, \pi]$ with $\boldsymbol{O'M} = R\boldsymbol{n}$ and $\boldsymbol{n} = \sin\theta\boldsymbol{e}_r + \cos\theta\boldsymbol{e}_z$. Consequently,

$$F_s = 2\pi R^2 \int_0^\pi \left\{\cos\theta\left[2\mu\frac{\partial w}{\partial z} - p\right] + \mu\sin\theta\left[\frac{\partial w}{\partial r} + \frac{\partial u_r}{\partial z}\right]\right\}\sin\theta\,\mathrm{d}\theta. \tag{2.8}$$

2.2. *Lubrication approximation and resulting problem for the pressure*

In our notation, the continuity equation in (2.1) becomes the linear relation

$$\frac{\partial w}{\partial z} = -\frac{1}{r}\frac{\partial}{\partial r}[ru_r], \tag{2.9}$$

while the momentum equation in (2.1) is nonlinear and thus much less tractable. Now, for a near-contact sphere the well-known lubrication approximation is relevant and makes it possible to solely retain the linear part of this equation. From the assumption that the sphere–slab gap δ is small compared with the sphere radius R, the classical (see Taylor, G. I., private communication cited in Handy & Bircumshaw 1925) lubrication analysis consists of asymptotically expanding in terms of the small parameter $\epsilon = \delta/R$ the flow velocity components (u_r, w) and pressure p in the vicinity of the origin O (recall figure 1), i.e. for $z = O(\delta)$ and $r = O(R)$. In the present paper the analysis is restricted to the first-order approximation. Let U and W denote the typical magnitudes of the velocity components u_r and u_z in the lubrication domain. The continuity equation (2.9) first gives $W = \epsilon U$. In approximating the momentum equation in (2.1) with boundary condition (2.3), the following Reynolds number Re_0 arises: $Re_0 = \rho|V_0 - V_p|\delta/\mu$. We assume that $\epsilon = \delta/R$ is small enough so that $Re_0 \ll 1$. Then, the nonlinear term on the left-hand side of the momentum equation (2.1) vanishes in the first approximation and, at the leading order in ϵ, this equation becomes

$$\frac{\partial p}{\partial r} = \mu\frac{\partial^2 u_r}{\partial z^2}, \quad \frac{\partial p}{\partial z} = 0. \tag{2.10a,b}$$

In the lubrication domain the following scalings, also obtained using (2.9)–(2.10), hold:

$$p \sim \mu\frac{U}{R}\left(\frac{R}{\delta}\right)^2, \quad \mu\frac{\partial w}{\partial z} \sim \mu\frac{W}{\delta} = \mu\frac{U}{R}, \quad \mu\frac{\partial w}{\partial r} \sim \mu\frac{\delta U}{R^2}, \quad \mu\frac{\partial u_r}{\partial z} \sim \mu\frac{U}{\delta}. \tag{2.11a–d}$$

In the lubrication approximation the leading contribution to the force F_s given by (2.8) is due to the part of the sphere located near the slab, i.e. to points of S for which $r = R\sin\theta$ with θ close to π. Furthermore, using (2.11) on the sphere boundary S shows that it is possible to retain only the pressure term on the right-hand side of (2.8). Upon performing the change of variable $r = r(\theta)$, and recalling from (2.10) that the pressure p is independent of z in the lubrication domain gives

$$F_s \sim 2\pi\int_0^{\mathcal{R}} p(r) r\,\mathrm{d}r. \tag{2.12}$$

In (2.12) the upper limit $\mathcal{R}$ is large compared with δ. It will be shown below, after (2.20), that the present (inner) expansion at scale δ is valid for $\mathcal{R} \to \infty$.

In summary, the task in this work reduces to the determination of the approximated lubrication pressure p and velocities (u_r, w) governed by the linear equations (2.9) and (2.7) and the far-field behaviour and boundary conditions (2.3)–(2.5).

The conditions (2.5) may be recast into the following form:

$$\frac{\partial u_r}{\partial z} = \lambda u_r \quad \text{for } z = 0, \quad \lambda = \frac{1}{l} = \frac{\sigma}{\sqrt{k^*}}. \tag{2.13a,b}$$

Now, the second equation (2.10) yields $p = p(r)$. Integrating twice the first equation (2.10) and taking into account (2.13) give the velocity profile

$$u_r(r, z) = [1 + \lambda z]u_r(r, 0) + \frac{z^2}{2\mu}\left[\frac{\mathrm{d}p}{\mathrm{d}r}\right](r). \tag{2.14}$$

At this stage the velocity $u_r(r, 0)$ on the interface is still unknown. It is obtained here by enforcing the boundary condition (2.3) on the sphere surface S in the radial direction. As shown in figure 1, this surface is described near the porous slab side by the equation $z = h(r)$. Therefore, equation (2.3) requires that $u_r(r, h) = 0$. With this condition the result for the radial velocity profile is

$$u_r(r, z) = \frac{1}{2\mu}\left[\frac{\mathrm{d}p}{\mathrm{d}r}\right](r)\left\{z^2 - h^2\left(\frac{\lambda z + 1}{\lambda h + 1}\right)\right\}. \tag{2.15}$$

Next, integrating the continuity equation (2.9) over z in $[0, h(r)]$ yields

$$w(r, h) = w(r, 0) - \frac{1}{r}\int_0^h \frac{\partial}{\partial r}[ru_r]\,\mathrm{d}z. \tag{2.16}$$

The boundary condition (2.3), when projected on the z direction, also provides $w(r, h) = V_0 - V_p$ while the first condition (2.4) gives $w(r, 0) = w'(r, 0)$. This latter quantity is given by the Darcy law (see first equation (2.2)), i.e. by $w'(r, 0) = -(k^*/\mu)(\partial p'/\partial z)_{z=0}$. As in Ramon *et al.* (2013), we assume a linear variation of the pressure p' across the slab: $(\partial p'/\partial z)_{z=0} \sim [p'(r, 0) - p'(r, -e)]/e$. As shown in appendix B, this assumption actually requires that $e \ll R$; that is, the porous slab thickness is small compared with the sphere radius. We also consider that the fluid below the slab imposes the pressure on the slab lower surface $\Sigma_l(z = -e)$, i.e. that $p'(r, -e) = 0$. Then we obtain the additional link $w'(r, 0) = -k^*p'(r, 0)/(\mu e)$. Noting that $p'(r, 0) = p(r, 0) = p(r)$, the combination of (2.16) and (2.15) provides the governing equation for the pressure p in the lubrication domain

$$\frac{1}{12\mu r}\frac{\mathrm{d}}{\mathrm{d}r}\left[\left\{\frac{(4 + \lambda h)h^3}{1 + \lambda h}\right\} r\frac{\mathrm{d}p}{\mathrm{d}r}\right] = V_0 - V_p + \frac{k^*p(r)}{\mu e}. \tag{2.17}$$

Equation (2.17) may be seen as an extension of the classical Reynolds equation (Reynolds 1886; Nguyen 2000). There is no mass injection on the $(O, \boldsymbol{e}_z)$ axis and thus $u_r'(r, 0) = 0$ at $r = 0$. By symmetry, $(\mathrm{d}p/\mathrm{d}r)(r = 0)$ vanishes. In addition p should vanish for large r. From the small normalized sphere–wall gap δ/R assumption, $h(r) \sim \delta + r^2/(2R)$ in the vicinity of the origin O, namely for $r \leqslant O(\sqrt{\delta R})$ as classically found. As in Ramon *et al.* (2013), we henceforth use the lengths (l_2, k) and the dimensionless parameter β, length s and pressure P such that

$$l_2 = \sqrt{2\delta R}, \quad k = \frac{k^*}{e}, \quad \beta = \frac{24kR}{\delta^2}, \quad s = \frac{r}{l_2}, \quad p = \frac{24\mu R}{\delta^2}(V_p - V_0)P. \tag{2.18a–e}$$

Henceforth, the reduced permeability β is simply called the permeability while k is the permeance. In addition, we also introduce the dimensionless sphere-to-slab gap $\tilde{\lambda}$:

$$\tilde{\lambda} = \lambda\delta = \delta/l = \frac{\sigma\delta}{\sqrt{k^*}}, \tag{2.19}$$

and then obtain for P the following dimensionless boundary value problem:

$$\frac{1}{s}\frac{\mathrm{d}}{\mathrm{d}s}\left\{\left[\frac{(4+\tilde{\lambda}H)H^3}{1+\tilde{\lambda}H}\right]s\frac{\mathrm{d}P}{\mathrm{d}s}\right\}-\beta P=-1,\quad \left(\frac{\mathrm{d}P}{\mathrm{d}s}\right)_{s=0}=P(\infty)=0, \tag{2.20a,b}$$

with $H=1+s^2$ the normalized sphere-to-wall distance at position s. The governing problem (2.20) extends that considered in Ramon *et al.* (2013) by applying the Saffman slip boundary condition. Not surprisingly, taking $\tilde{\lambda}\to\infty$ in (2.20) recovers the Ramon formulation.

The problem (2.20) is well-posed for large s as may be proven by considering its asymptotic expansion for $s\gg 1$. Then $H\sim s^2$ and the differential equation may be recast in terms of the variable H

$$4\frac{\mathrm{d}}{\mathrm{d}H}\left(H^4\frac{\mathrm{d}P}{\mathrm{d}H}\right)-\beta P=-1. \tag{2.21}$$

For $H\gg 1$ the first term takes over and the formal solution behaves like $P\sim H^{-2}\sim s^{-4}$. Thus, the condition at infinity in (2.20) can indeed be applied and the lubrication problem is regular as expected. Moreover, in the integral (2.12) for the force F_s the upper limit $\mathcal{R}$ is rejected to infinity.

As in Ramon *et al.* (2013), the force F_s is normalized by that obtained for an impermeable no-slip wall. Using our previous scalings (2.11) and (2.18) for s and P, the normalized force F is

$$F=\frac{\delta F_s}{6\pi\mu(V_p-V_0)R^2}=16\int_0^\infty P(s)s\,\mathrm{d}s. \tag{2.22}$$

In this paper we focus on the normalized force F which, by virtue of (2.19)–(2.22), depends on the sphere–slab gap δ, the sphere radius R and the porous slab properties (k^*, e, σ) through the dimensionless parameters β and $\tilde{\lambda}$. The validity of the present formulation however brings some additional restrictions to the previously mentioned ones in (2.6). First, we must recall the condition, discussed after (2.16), of a sufficiently thin slab with $e\ll R$. Second, the lubrication approximation is valid for $r\leqslant O(l_2)$ and the associated domain on the upper slab boundary $z=0$ must contain a large number of pores, i.e. $r_p=\sqrt{k^*}\ll l_2$. In summary, we require in the present paper that for a slip porous slab

$$\sigma\geqslant 0,\quad \sqrt{k^*}\ll e\ll R,\quad \sqrt{k^*}\ll\sqrt{\delta R}. \tag{2.23a–c}$$

The particular value $\sigma=\infty$ is here employed with $k^*>0$ to retrieve the no-slip permeable slab (case $l=0$) handled in Ramon *et al.* (2013).

2.3. *Numerical implementation and tests*

For the no-slip permeable slab case (Saffman case with $\tilde{\lambda}=\infty$) the solution of (2.20) for the lubrication pressure P is obtained in closed form. This solution, surprisingly not reported in Ramon *et al.* (2013), is given in appendix A. In all other cases, equation (2.20) has to be solved numerically. This is achieved using a truncated domain $0\leqslant s\leqslant L$ and a $O(h^2)$ second-order finite-difference scheme with $N+1$ nodal points $s_n=nh$ (taking $n=0,1,\ldots,N$) and $h=L/N$. We then calculate the

normalized force F taking as L the upper value of the domain of integration in the integral occurring on the right-hand side of (2.22). This procedure is benchmarked for $\beta = 1, 100$ against the force obtained for the no-slip permeable case. That force is obtained here by integrating, using Maple computer algebra software and taking $L = \infty$, the product $P(s)s$ with P the analytical lubrication pressure displayed in appendix A.

As shown in table 1, the numerical results converge as L increases and become very close to the analytical results. In view of these results we henceforth take $L = 80$ which is sufficient for a three-digit accuracy.

3. Results for the pressure field and drag force

The normalized force, F, solely depends upon the positive dimensionless permeability β and slip parameter $\tilde{\lambda}$ given by

$$\beta = 24\left(\frac{k}{R}\right)\left(\frac{R}{\delta}\right)^2, \quad \tilde{\lambda} = \frac{\delta}{l} = \left(\frac{\delta}{R}\right)\Big/\left(\frac{l}{R}\right). \tag{3.1a,b}$$

In practice, these parameters take values in the interval $[\,0, \infty\,[$.

3.1. *Asymptotic expansion for* $\beta \gg 1$

As achieved in Ramon *et al.* (2013) for the no-slip case, it is worth estimating for the Saffman slip case the resulting normalized lubrication pressure P and force F for either large or small values of the permeability β. In this subsection we consider the case of a sphere translating towards a near-contact permeable slab ($k = k^*/e > 0$) in the limit $\beta \gg 1$ of large permeability. In such circumstances asymptotic expansions for P and F can be derived by extending the treatment proposed in Ramon *et al.* (2013). Curtailing the details, the pressure P takes, for β large, the following form:

$$P(s) = \frac{P^*(\eta)}{\beta}, \quad \eta = \frac{s}{\beta^{1/4}}, \quad P^*(\eta) \sim P_0^*(\eta) + \frac{P_1^*(\eta)}{\beta^{1/2}} + \frac{P_2^*(\eta)}{\beta}, \tag{3.2a–c}$$

with, using Maple software, the functions

$$P_0^*(\eta) = 1 - \left[\frac{1+2\eta^2}{2\eta^2}\right] \mathrm{e}^{-1/(2\eta^2)}, \quad P_1^*(\eta) = -\frac{3}{16}\left[\frac{1+\tilde{\lambda}}{\tilde{\lambda}\eta^6}\right] \mathrm{e}^{-1/(2\eta^2)}, \tag{3.3a,b}$$

$$\begin{aligned} P_2^*(\eta) \;=\; & -\frac{1}{256\eta^{10}}\left[9 - 58\eta^2 + 4\eta^4 + \frac{1}{\tilde{\lambda}}(18 - 116\eta^2 + 8\eta^4)\right. \\ & \left. + \frac{1}{\tilde{\lambda}^2}(9 + 122\eta^2 + 68\eta^4)\right] \mathrm{e}^{-1/(2\eta^2)}. \end{aligned} \tag{3.4}$$

Of course, letting $\tilde{\lambda}$ tend to infinity in (3.2)–(3.4) retrieves the asymptotics given in Ramon *et al.* (2013). Observe that for (3.2) to be an asymptotic expansion, $\tilde{\lambda}$ cannot vanish (inspect P_1^* in (3.3) and P_2^* in (3.4)). In practice, the expansion (3.2) is valid for $\sqrt{\beta} \gg \mathrm{Max}(1, \tilde{\lambda}^{-1})$. On the basis of (3.2)–(3.4), an asymptotic expansion is derived for the dimensionless drag force from (2.22):

$$F \sim \frac{4}{\beta^{1/2}} - \left[\frac{6(\tilde{\lambda}+1)}{\tilde{\lambda}}\right]\frac{1}{\beta} + \frac{3}{2}\left[\frac{17 + \tilde{\lambda}(2+\tilde{\lambda})}{\tilde{\lambda}^2}\right]\frac{1}{\beta^{3/2}} \quad \text{for } \sqrt{\beta} \gg \mathrm{Max}(1, \tilde{\lambda}^{-1}). \tag{3.5}$$

L	50	80	100	200	∞
$F, \beta = 1$	0.95996	0.96045	0.96056	0.96071	0.96077
$F, \beta = 100$	0.34087	0.34136	0.34147	0.34162	0.34167

TABLE 1. Normalized force F versus the length L for the no-slip permeable case (i.e. as in Ramon *et al.* (2013)) and $\beta = 1, 100$. For $L < \infty$ the lubrication pressure is calculated numerically by solving (2.20) for the Saffman boundary condition ($\delta_{BJ} = 0$) and $\tilde{\lambda} \to \infty$. The last column for $L = \infty$ is the analytical lubrication pressure given in appendix A.

Let us introduce the dimensionless permeability $\bar{k} = 24k/R = 24k^*/(eR) > 0$ which compares the porous slab typical pore size $r_p = \sqrt{k^*}$ with the length $\sqrt{eR}$. From our second assumption (2.23), it turns out that $k^* \ll eR$, i.e. that $\bar{k} \ll 24$. The requirement $\sqrt{\beta} \gg \mathrm{Max}(1, \tilde{\lambda}^{-1})$ then becomes $\sqrt{\bar{k}} \gg \mathrm{Max}(\delta/R, l/R)$. These constraints tell us to what extent the ratio $k^*/(eR)$ must be large enough for given parameters $(\delta/R, l/R)$. Using (2.22) and (3.5) provides the following approximation of the dimensional force F_s experienced by a sphere translating normal and very close to a permeable (porous) slab with upper surface subject to the Saffman condition:

$$F_s \sim 6\pi\mu(V_p - V_0)R \left\{ \frac{4}{(\bar{k})^{1/2}} - \frac{6(\tilde{\lambda}+1)}{\tilde{\lambda}\bar{k}} \left(\frac{\delta}{R}\right) + \frac{3}{2(\bar{k})^{3/2}} \left[\frac{17 + \tilde{\lambda}(2+\tilde{\lambda})}{\tilde{\lambda}^2}\right] \left(\frac{\delta}{R}\right)^2 \right\} \quad \text{for } \sqrt{\bar{k}} \gg \mathrm{Max}(\delta/R, l/R). \tag{3.6}$$

According to (3.2)–(3.6), the first approximations of the lubrication pressure and of the resulting force exerted on a sphere close to the permeable ($k > 0$) porous slab are independent of the slip parameter $\tilde{\lambda}$. For a large permeability this was not *a priori* expected on physical grounds. The Saffman condition is found to affect the lubrication pressure and dimensional force only at the next order.

The range of validity of the asymptotic expansion (3.5) is evaluated by comparing in table 2 its predictions against the numerical results of three-digit accuracy . Clearly, the asymptotic expansion does not actually hold for $\tilde{\lambda} = 1$ when $\beta = 10, 50$. (This is actually still the case when $\tilde{\lambda} = 0.1$ for $\beta = 1000$ with $F = 0.0930$ and $F_a = 0.1421$ and also for $\beta = 5000$ with $F = 0.0474$ and $F_a = 0.0507$. In contrast, for $\tilde{\lambda} = 0.1$ and $\beta = 10\,000$ the closer values $F = 0.0348$ and $F_a = 0.0360$ are obtained.) However, as seen in table 2, the asymptotic expansion provides already for $\beta = 50$ and $\tilde{\lambda} \geqslant 10$ the same three-digit accuracy and may therefore be seen as a handy formula in the range $\beta \geqslant 50$ for this domain of the slip parameter $\tilde{\lambda}$. It also nicely matches the numerics for $\tilde{\lambda} \geqslant 1$ when $\beta \geqslant 100$.

3.2. *Asymptotic expansion for* $\beta \ll 1$

For a vanishing porous slab permeance $k = k^*/e$, the dimensionless permeability β might be small compared with unity even for a very small normalized sphere–slab gap δ/R (see (2.23)). More precisely, since $\beta = \bar{k}(R/\delta)^2$ the condition $\beta \ll 1$ is ensured for $\sqrt{\bar{k}} \ll \delta/R$. In such circumstances a regular expansion of the problem (2.20) for

	$\tilde{\lambda}=1$		$\tilde{\lambda}=10$		$\tilde{\lambda}=100$		$\tilde{\lambda}=1000$	
β	F	F_a	F	F_a	F	F_a	F	F_a
* 0.01	0.6290	0.6293	0.9156	0.9159	0.9895	0.9898	0.9983	0.9986
0.01	0.6290	0.6293	0.9156	0.9159	0.9895	0.9898	0.9983	0.9986
* 0.1	0.6279	0.6283	0.9127	0.9130	0.9858	0.9863	0.9945	0.9948
0.1	0.6279	0.6283	0.9127	0.9130	0.9858	0.9862	0.9945	0.9949
* 0.7	0.6210	0.6212	0.8941	0.8937	0.9627	0.9619	0.9708	0.9699
0.7	0.6210	0.6214	0.8941	0.8945	0.9627	0.9631	0.9708	0.9708
* 1	0.6177	0.6177	0.8853	0.8840	0.9517	0.9498	0.9596	0.9575
1	0.6177	0.6180	0.8853	0.8857	0.9517	0.9522	0.9596	0.9593
10	0.5376	1.0136	0.7030	0.6699	0.7358	0.7074	0.7394	0.7118
50	0.3784	0.4105	0.4400	0.4395	0.4493	0.4488	0.4503	0.4498
100	0.3004	0.3100	0.3359	0.3361	0.3408	0.3409	0.3413	0.3414

TABLE 2. Computed normalized force in the Saffman case, F, for a large range of values of the dimensionless permeability, β, and asymptotic estimate, F_a, for either $\beta \gg 1$ (§ 3.1) or $\beta \ll 1$ (§ 3.2), both for various values of the parameter $\tilde{\lambda}$ (see (2.19)). The asymptotic values F_a for $\beta \leqslant 1$ have been obtained using the small β approximation given in § 3.2. Each line with a $*$ symbol reports the closed-form (order $O(\beta)$) approximation in small β obtained by retaining only the first two terms in (3.10).

small β is worked out, as also done in Ramon *et al.* (2013) for the no-slip case. Omitting the details, the pressure P is approximated as

$$P(s) = P_0(s) + \beta P_1(s) + \beta^2 P_2(s) + O(\beta^3) \quad \text{for } \beta \ll 1, \tag{3.7}$$

with the zeroth-order pressure P_0 and first-order pressure P_1 derived in closed form (again using the Maple software), that is

$$P_0(s) = \frac{3\tilde{\lambda}^2}{256} \log\left[\frac{\tilde{\lambda}(1+s^2)}{4+\tilde{\lambda}(1+s^2)}\right] + \frac{2+3\tilde{\lambda}(1+s^2)}{64(1+s^2)^2} \tag{3.8}$$

and a much more complicated form for P_1 given in appendix C. Finally, the second-order pressure P_2 was calculated numerically using a finite-difference scheme (as in § 2.3) to solve the following problem (from the extended Reynolds equation (2.20)):

$$\frac{1}{s}\frac{\mathrm{d}}{\mathrm{d}s}\left\{\left[\frac{(4+\tilde{\lambda}H)H^3}{1+\tilde{\lambda}H}\right] s\frac{\mathrm{d}P_2}{\mathrm{d}s}\right\} = P_1, \quad \left(\frac{\mathrm{d}P_2}{\mathrm{d}s}\right)_{s=0} = P_2(\infty) = 0. \tag{3.9a,b}$$

Following (3.7) and applying (2.22), the expansion for the normalized force F reads

$$F = F_0(\tilde{\lambda}) + \beta F_1(\tilde{\lambda}) + \beta^2 F_2(\tilde{\lambda}) + O(\beta^3) \quad \text{for } \beta \ll 1. \tag{3.10}$$

Although the analytical expression for the pressure P_1 is very involved (see appendix C), it is nevertheless possible to find a simple expression for $F_1(\tilde{\lambda})$. The results are

$$F_0(\tilde{\lambda}) = \frac{1}{8}(2-3\tilde{\lambda}) + \frac{3\tilde{\lambda}}{32}(4+\tilde{\lambda})X, \quad X = \log\left(\frac{4+\tilde{\lambda}}{\tilde{\lambda}}\right), \tag{3.11a,b}$$

$$F_1(\tilde{\lambda}) = -\frac{1}{384} - \frac{3\tilde{\lambda}}{256} - \frac{3\tilde{\lambda}^2(4-X)}{512} + \frac{3\tilde{\lambda}^3 X}{2048}[1+3X] + \frac{9\tilde{\lambda}^4 X^2}{8192}. \tag{3.12}$$

By inspection of (3.11)–(3.12) and as shown in figure 2 it is observed that both coefficients F_0 and F_1 remain of the order of unity in the entire range $\tilde{\lambda} \geqslant 0$.

It should be noted that $F_0(\tilde{\lambda})$ is actually the normalized force experienced by a sphere located close to (i.e. in the lubrication regime $\delta \ll R$) an impermeable surface on which the usual Navier slip condition holds. In this case the result (3.11) is recovered from Vinogradova (1995) lubrication analysis (see equations (3.18)–(3.19) there), by letting in her notation $R_2 \to \infty$, $b \to 0$ and $k \to \infty$ with $kb = l$ being the slip length. We used Maple computer algebra software to check this limit. In principle, we should also retrieve the function $F_0(\tilde{\lambda})$ from Goren (1973) lubrication results (his equation (17)), converting his notation with $Kn_s = l/R$, $h = \delta$ and $Kn_w \to 0$. (We could not however succeed in retrieving his result and suspect a misprint in his equation (17) for two reasons: first, there are two analogous terms $4ST$ and $2ST$ in the same parentheses and, second, his results from table 1 are not recovered from his formula (17).)

As $\tilde{\lambda}$ becomes large the no-slip boundary condition applies and the zeroth-order pressure P_0 tends to the function obtained in Ramon *et al.* (2013) while $F_0(\tilde{\lambda}) \sim 1$ and $F_1(\tilde{\lambda}) \sim -1/24$. We also recover the results by Goren (1979) for a very thin membrane.

Like P_0 and P_1, the pressure P_2 solution of (3.9) is of order unity whatever the value of $\tilde{\lambda} \geqslant 0$. Therefore, and in contrast to the previous case of large permeability β, no restriction bearing on the slip parameter $\tilde{\lambda}$ appears here for the expansions (3.7) and (3.10) to be valid. Again invoking (2.22) eventually provides the following expansion for the dimensionless force:

$$\begin{aligned} F_s \;=\; 6\pi\mu(V_p - V_0)R \Bigg\{ & F_0(\tilde{\lambda}) \left(\frac{R}{\delta}\right) + F_1(\tilde{\lambda})\bar{k} \left(\frac{R}{\delta}\right)^3 \\ & + F_2(\tilde{\lambda})\bar{k}^2 \left(\frac{R}{\delta}\right)^5 + O\left(\bar{k}^3 \left(\frac{R}{\delta}\right)^7\right) \Bigg\} \quad \text{for } \beta \ll 1. \end{aligned} \tag{3.13}$$

As for the case of large permeability, the asymptotic estimate (3.10) of the normalized force F for $\beta \ll 1$ was tested against the numerical predictions. The results displayed in table 2 show the approximation (3.10) both at $O(\beta^2)$ 'first order' and $O(\beta^3)$ 'second order'. From table 2 the agreement between the three-digit numerics and both (first-order and second-order) asymptotic approximations for the normalized force turns out to be amazingly good (that is, within $O(10^{-4})$ accuracy) up to $\beta = 0.1$ in the entire range $\tilde{\lambda} \geqslant 1$. Note also that the first-order approximation, obtained by retaining the first two terms on the right-hand side of (3.10), may be considered as a handy formula for practical use.

3.3. *Numerical results*

In practice the permeability parameter β can take values in the entire range $\beta \geqslant 0$. For β neither small nor large the lubrication pressure P and resulting normalized force F have to be calculated numerically. This is achieved in the present work, with a three-digit accuracy, using the numerical method described in § 2.3.

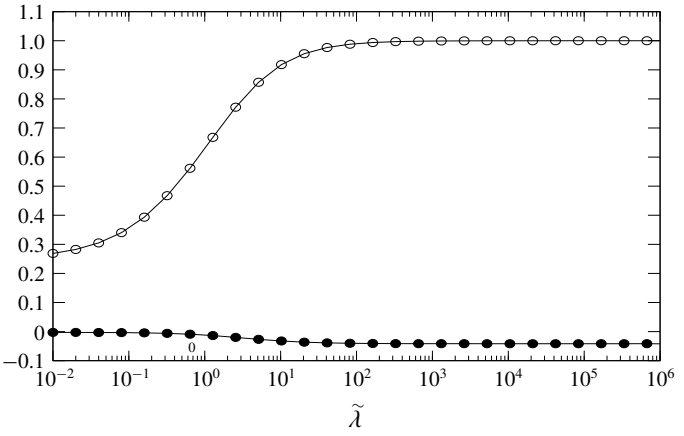

FIGURE 2. Coefficients F_0 (○) and F_1 (●) of the normalized force, see (3.11) and (3.12), versus $\tilde{\lambda}$ for low dimensionless permeability, $\beta \ll 1$.

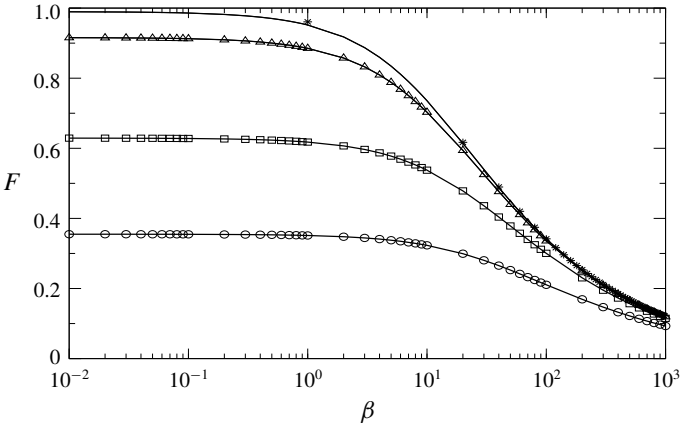

FIGURE 3. Normalized force F versus the permeability parameter β for $\tilde{\lambda}=0.1$ (○), $\tilde{\lambda}=1$ (□), $\tilde{\lambda}=10$ (△) and $\tilde{\lambda}=100$ (solid curve). For comparison purposes, a few values obtained for the no-slip Ramon case (associated with $\tilde{\lambda}=\infty$) are also indicated by $*$ symbols.

Figure 3 displays the force F versus β in the range $[0.01, 1000]$ for the Saffman slip case $\tilde{\lambda}=0.1, 1, 10, 100$ and also for the Ramon no-slip case (associated with the value $\tilde{\lambda}=\infty$). The slip parameter is also written $\tilde{\lambda}=\delta/l$ with l the porous slab slip length. The curves in figure 3 reveal that F is deeply sensitive to the ratio δ/l in a wide range (say here in the range $[0.01, 100]$) of the permeability β. Not surprisingly, at given values of β and of the small sphere–slab gap δ, the normalized force decreases as the slip increases (i.e. as l increases). Moreover, at given slip parameter $\tilde{\lambda}$ the force quickly reaches for $\beta \leqslant O(1)$ its limit value for the impermeable ($\beta=0$) slab case. This limit value agrees with the one obtained by Vinogradova (1995) for the impermeable slipping wall case. Of course, as shown by the leading order in expansion (3.5), all curves collapse as β becomes large enough. Moreover, it is observed in figure 3 that curves for $\tilde{\lambda} \geqslant 1$ almost coincide as soon as $\beta \geqslant 1000$.

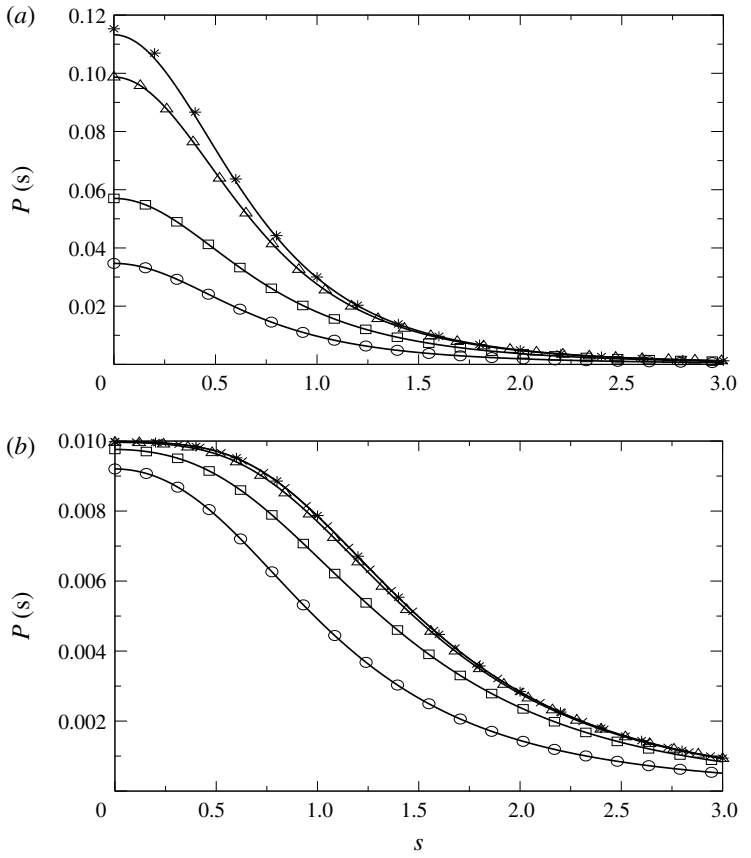

FIGURE 4. Lubrication pressure P versus s for $\tilde{\lambda}=0.1$ (○), $\tilde{\lambda}=1$ (□), $\tilde{\lambda}=10$ (△), $\tilde{\lambda}=100$ (solid curve) and also for the $\tilde{\lambda}=\infty$ case (no curve but $*$ symbols). (*a*) Case $\beta=1$. (*b*) Case $\beta=100$.

The lubrication pressure $P(s)$ is also displayed in figure 4 versus the normalized radial coordinate in the gap, s, for $\beta=1, 100$ and the same values of $\tilde{\lambda}$ as in figure 3. As shown for $\beta=1$ in figure 4(*a*), the pressure is strongly sensitive to the value of $\tilde{\lambda}$ but is mainly exerted in the narrow domain $s\leqslant 1.5$ close to the symmetry axis. In contrast, figure 4(*b*) reveals that for $\beta=100$ the pressure becomes less sensitive to the parameter $\tilde{\lambda}$ but is mainly distributed in the extended range $s\leqslant 3$.

4. Settling of a solid sphere near a porous slab

This section considers the settling of a solid sphere towards a near-contact porous slab. There is no background permeation ($V_0=0$) and the uniform gravity field $\boldsymbol{g}=-g\boldsymbol{e}_z$ is normal to the slab.

4.1. *Time-dependent problem and numerical treatment*

As displayed in figure 1, the sphere centre is O' with $\boldsymbol{OO'}=(R+\delta)\boldsymbol{e}_z$. The sphere–slab gap δ now depends on time t. The sphere density ρ_s is uniform, so that the sphere settles without rotating at the translational velocity $-V_p\boldsymbol{e}_z$ with $V_p=-\mathrm{d}\delta/\mathrm{d}t$. Since the

$\bar{t}$	1	2	3	5	10
Analytical	0.08840	0.03907	0.01727	0.003373	0.0000569
Numerical (i)	0.08840	0.03907	0.01727	0.003373	0.0000569
Numerical (ii)	0.08837	0.03905	0.01725	0.003369	0.0000568
Numerical (iii)	0.08837	0.03905	0.01725	0.003369	0.0000568

TABLE 3. Analytical and numerical values of normalized sphere–slab gap $\bar{\delta} = \delta/R$ at different dimensionless times $\bar{t} = 1, 2, 3, 5, 10$ in the impermeable ($\beta = 0$) and no-slip ($\tilde{\lambda} = \infty$) case. Here $\bar{\delta}_0 = 0.2$ and (4.2) is solved numerically by the marching-in-time algorithm taking for the dimensionless force F either (i) its analytical value $F = 1$; or (ii) its numerical Ramon value (as in table 1); or (iii) its numerical value calculated for the Saffman condition with $\tilde{\lambda} = \infty$.

fluid has a uniform density ρ the sphere buoyancy-corrected mass is $m = 4\pi(\rho_s - \rho)R^3/3$. Accounting for gravity, the flow field perturbed by the sphere is $(\boldsymbol{u}, p + \rho \boldsymbol{g}\cdot\boldsymbol{x})$ in the fluid domain $\mathcal{D}$ and $(\boldsymbol{u}', p' + \rho \boldsymbol{g}\cdot\boldsymbol{x})$ in the slab $\mathcal{S}$ with $(\boldsymbol{u}, p)$ and $(\boldsymbol{u}', p')$ still governed by (2.2)–(2.5) and the lubrication approximation (2.10). The total (hydrodynamic plus gravity) force exerted on the sphere with volume $\mathcal{V}$ is $(F_s + \rho\mathcal{V}g)\boldsymbol{e}_z$ where F_s is related to the normalized force F by (2.22) (in which one sets $V_0 = 0$). Neglecting the sphere inertia, which corresponds to either a liquid or a gas at low Stokes number, the time-dependent sphere 'location' $\delta(t)$ is the solution to the following problem:

$$\frac{\mathrm{d}\delta}{\mathrm{d}t} = -\frac{mg\delta}{6\pi\mu R^2 F}, \quad \delta(t=0) = \delta_0, \tag{4.1a,b}$$

with δ_0 the prescribed initial sphere–slab gap.

As outlined after (2.22), the normalized force F solely depends upon δ/R and the dimensionless parameters $(\beta, \tilde{\lambda})$. From the definitions (3.1), the time-dependent normalized sphere 'location' $\bar{\delta} = \delta/R$ is thus determined by the time scale $\tau_g = \sqrt{24}\pi\mu R^2/(mg)$ as in Ramon *et al.* (2013), the given initial sphere location $\bar{\delta}_0 = \delta_0/R$ and the auxiliary parameters $(k/R, l/R)$. For convenience, the normalized time $\bar{t} = t/\tau_g$ is introduced. From (4.1), we obtain the ratio $\bar{\delta}$ versus $\bar{t}$, for given quantities $(\bar{\delta}_0, k/R, l/R)$, by solving the problem

$$\frac{\mathrm{d}\bar{\delta}}{\mathrm{d}\bar{t}} = -\left[\frac{(2/3)^{1/2}}{F}\right]\bar{\delta}, \quad \bar{\delta}(\bar{t}=0) = \bar{\delta}_0. \tag{4.2a,b}$$

Except for a no-slip and impermeable slab (see below), this task requires a numerical procedure. In the present work we resort to a predictor–corrector marching-in-time algorithm (except for the first two time steps for which a second-order Runge–Kutta scheme is used) to solve (4.2). This procedure is benchmarked against the analytical solution available for a no-slip and impermeable slab (i.e. for the case of a usual no-slip solid boundary wall Σ_u). Indeed, in such circumstances $k = \beta = 0$ while $\tilde{\lambda} \to \infty$ so that (recall (3.10) and our discussion after (3.12)) $F = 1$ whatever $\bar{\delta}$. Analytically solving (4.2) thus becomes possible and yields the analytical solution $\bar{\delta}_a = \bar{\delta}_0 \mathrm{e}^{-\sqrt{2/3}\bar{t}}$.

As shown in table 3, the analytical solution $\bar{\delta}_a$ is accurately retrieved by the numerics.

k/R	l/R	$\overline{k}^{1/2}$	β_1	β_2	β_3	$\tilde{\lambda}_1$	$\tilde{\lambda}_2$	$\tilde{\lambda}_3$
1×10^{-5}	—	1.55×10^{-2}	2.4×10^{-2}	2.4	240	—	—	—
1×10^{-4}	—	0.049	0.24	24	2400	—	—	—
1×10^{-3}	—	0.155	2.4	240	24 000	—	—	—
1×10^{-2}	—	0.490	24	2400	240 000	—	—	—
—	1×10^{-3}	—	—	—	—	100	10	1
—	1×10^{-2}	—	—	—	—	10	1	0.1
—	1×10^{-1}	—	—	—	—	1	0.1	0.01

TABLE 4. Values of $\overline{k}^{1/2}$, β and $\tilde{\lambda}$ for different parameters k/R, l/R and normalized gap $\overline{\delta}$. Here β_n and $\tilde{\lambda}_n$ are obtained for $\overline{\delta}=10^{-n}$ with $n=1, 2, 3$.

We compute the sphere trajectory $\overline{\delta}(\bar{t})$ for prescribed sphere initial location $\overline{\delta}_0$ and parameters $(k/R, l/R)$. Both parameters β and $\tilde{\lambda}$ evolve on the trajectory with, as the sphere approaches the slab, an increase of β and a decrease of $\tilde{\lambda}$. The product $C=\beta\tilde{\lambda}^2/24=(k/R)/(l/R)^2\geqslant 0$ is however constant on each trajectory with a value entirely prescribed by the parameters $(k/R, l/R)$ (i.e. indepently of the initial location $\overline{\delta}_0$).

For a permeable slab (that is, for a positive slab permeance ratio k/R), note that $\beta\to\infty$ as the sphere approaches the slab. Moreover, for a sufficiently small sphere–slab normalized gap $\overline{\delta}$ then $\sqrt{\beta}$ becomes large enough for (3.5) to hold with $F\sim 4\beta^{-1/2}=(2/3)^{1/2}(k/R)^{-1/2}\overline{\delta}$ and the sphere normalized velocity $[\mathrm{d}\overline{\delta}/\mathrm{d}\bar{t}]\boldsymbol{e}_z$ therefore adopts the time-independent value $-V_{pc}\boldsymbol{e}_z$ with $V_{pc}=\sqrt{k/R}$. As found in § 3.1, the sphere velocity V_p tends to V_{pc} for $\sqrt{\overline{k}}\gg \mathrm{Max}(\overline{\delta}, l/R)$ with $\overline{k}=24k/R$.

4.2. *Settling trajectories*

The sphere trajectory sensitivity to the parameters k/R and l/R is illustrated in figure 5 which plots $\overline{\delta}$ versus $\bar{t}$ for the initial location $\overline{\delta}_0=0.2$ and various values of the permeability parameter $k/R=0.001, 0.01$ and of the slip parameter $l/R=0, 0.01, 0.1$.

As expected, the sphere settles faster towards a porous slab than towards a no-slip impermeable (dashed line) plane wall. In addition, for a given value of k/R the sphere approaches faster the slap as the slip parameter l/R increases. Trajectories for a slipping slab either for $l/R=0.01$ or $l/R=0.1$ differ either weakly or moderately, respectively, from the one prevailing in the no-slip case (see Ramon *et al.* 2013). Moreover, these differences decrease in magnitude as k/R increases.

The slopes of trajectories for slip and no-slip porous slabs approach each other as $\overline{\delta}$ decreases. This can be observed by tracking on a trajectory for given $l>0$ the slope ratio (see (4.2)) $s_r(\overline{\delta})=F(\infty,\beta)/F(\tilde{\lambda},\beta)>1$ versus the pair $(\tilde{\lambda},\beta)$ which evolves as $\overline{\delta}$ drops. This can be done using table 4 and then figure 3.

Hence, for the $l/R=0.1$ trajectory in figure 5(*a*) note that, from table 4, $(\tilde{\lambda},\beta)=(\tilde{\lambda}_1,\beta_1)=(1, 2.4)$ for $\overline{\delta}=0.1$ and $(\tilde{\lambda},\beta)=(\tilde{\lambda}_2,\beta_2)=(0.1, 240)$ for $\overline{\delta}=0.01$. From inspection of figure 3, it thus follows that $s_t(\overline{\delta}_1)>s_t(\overline{\delta}_2)$.

As predicted at the end of § 4.1, each trajectory slope tends to the time-independent limit $-V_{pc}$ for $\overline{\delta}$ sufficiently small in the following sense: $\sqrt{\overline{k}}\gg\mathrm{Max}(\overline{\delta}, l/R)$. This trend is checked by also plotting in figure 5(*a*,*b*) the fictitious straight trajectory Λ of a sphere that would settle with the previous time-independent velocity $V_{pc}=\sqrt{k/R}$.

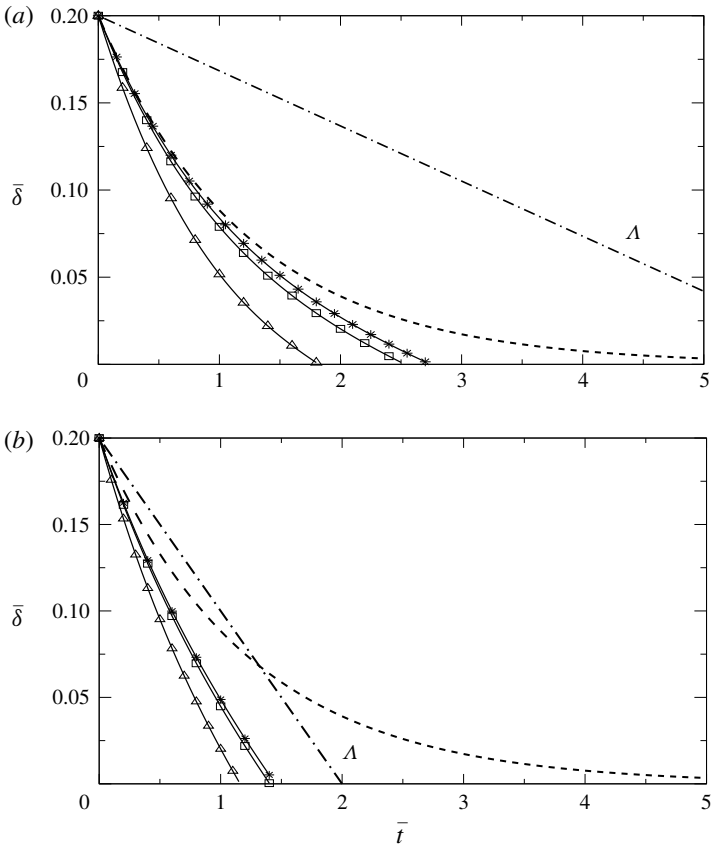

FIGURE 5. Normalized sphere–slab gap $\bar{\delta}$ versus dimensionless time $\bar{t}$ for a no-slip and impermeable ($k/R = 0$) slab (dashed curve) and for a permeable slab, with either $k/R = 0.001$ (*a*) or $k/R = 0.01$ (*b*). The permeable slab is either no-slip with $l/R = 0$ ($*$) or slipping with the Saffman boundary condition with normalized slip length $l/R = 0.01$ ($\square$) and $l/R = 0.1$ ($\triangle$). Here $\bar{\delta}_0 = 0.2$ and the fictitious straight trajectory Λ (see § 4.1) of a sphere settling at the constant velocity $-V_{pc}\boldsymbol{e}_z$ is also displayed (straight dash-dotted line).

For $\bar{\delta} \sim 0.01$ the slopes of Λ and the trajectories for a permeable slab become close for $k/R = 0.001$ and very close for $k/R = 0.01$, respectively. This is because, as shown in table 4, the condition $\sqrt{\bar{k}} \geqslant \mathrm{Max}(0.01,\, l/R)$ or $\sqrt{\bar{k}} \gg \mathrm{Max}(0.01,\, l/R)$ is met for $k/R = 0.001$ or $k/R = 0.01$, respectively.

5. Conclusions

The governing problem for the pressure exerted on a sphere translating towards a porous slab at close range is solved within the lubrication approximation using also the assumption of a thin slab. This latter assumption makes it possible to circumvent the determination of the flows inside and below the slab. Using the Saffman slip boundary condition on the porous slab upper interface, the pressure is obtained by solving a Reynolds-like equation and the drag force is obtained therefrom. These quantities solely depend on the dimensionless permeability $\beta = 24kR/\delta^2$ and sphere–slab gap parameter $\tilde{\lambda} = \delta/l$.

Handy formulae are proposed for the normalized force at large and small permeability β. These formulae agree well with the computed results which are valid in the entire range $\beta > 0$.

For vanishing permeability β our asymptotics retrieve the result of Vinogradova (1995) whatever the slip length. For small permeability β and a vanishing slip length our asymptotic results agree with those of Ramon *et al.* (2013).

Based on the preceding results, the sphere settling trajectory is found to depend significantly upon the slip length ratio l/R, especially at low permeance ratio (low k/R).

This work is restricted to the analysis of a thin slab ($e/R \ll 1$) therefore simplifying the flow field in the slab and disregarding that below the slab. It would be useful to relax this thin-slab condition. This task however requires the determination of the axisymmetric Stokes flows above and below the slab, coupled with the Darcy flow in the slab through the Saffman slip condition on both permeable interfaces. This challenging issue is therefore postponed to another work.

Appendix A. Closed-form lubrication pressure for the permeable no-slip thin-slab case

The case of the no-slip thin permeable slab, handled in Ramon *et al.* (2013), is obtained using the Saffman slip condition with $\tilde{\lambda} = \infty$. Setting $v = [\beta s^2/(1+s^2)]^{1/2}$ and using Maple software, the lubrication pressure $P(s)$ solution to (2.20) in this case is found to be

$$P(s) = \frac{[v(1+s^2)]^{-1}}{2\beta I_1(\sqrt{\beta})} \left\{ 2s^2[I_1(\sqrt{\beta})v - \sqrt{\beta} I_1(v)] + v[2I_1(\sqrt{\beta}) - \sqrt{\beta} I_0(v)] \right\}, \quad \text{(A 1)}$$

with I_0 and I_1 the usual modified Bessel functions (of the first kind) of zeroth and first order, respectively (see Abramowitz & Stegun (1965)).

Appendix B. Approximation of $(\partial p'/\partial z)_{z=0}$ for a thin porous slab

Using a Taylor expansion of the pressure $p'(r, z)$ in the porous slab yields the approximation

$$p'(r, -e) = p'(r, 0) - e \left(\frac{\partial p'}{\partial z} \right)_{z=0} + \frac{e^2}{2} \left(\frac{\partial^2 p'}{\partial z^2} \right)_{z=0} + \cdots . \quad \text{(B 1)}$$

From equations (2.2), it is classical that p' is harmonic in the porous slab. With our cylindrical coordinates (r, z) this property reads

$$\left(\frac{\partial^2 p'}{\partial z^2} \right) = -\frac{1}{r} \frac{\partial}{\partial r} \left[r \frac{\partial p'}{\partial r} \right]. \quad \text{(B 2)}$$

If p' scales like P' in the slab, in which r has typical size R, the scale of the last term in (B 1) is thus $e^2 P'/R^2$. Accordingly, for $e \ll R$ the expansion (B 1) becomes, as discussed after (2.16), $(\partial p'/\partial z)_{z=0} \sim [p'(r, 0) - p'(r, -e)]/e$.

Appendix C. Pressure term P_1 for vanishing β

Defining the dilogarithmic function dilog as (Abramowitz & Stegun 1965)

$$\mathrm{dilog}(x) = \int_1^x \frac{\log t \, \mathrm{d}t}{1-t} \tag{C 1}$$

and setting $u = s^2$, the pressure term P_1 is found by running Maple software to take the following form:

$$\begin{aligned} P_1(s) \;=\; & \frac{3\tilde{\lambda}(1+\tilde{\lambda})}{1024}[\mathrm{dilog}(H) - \mathrm{dilog}(1+\tilde{\lambda}H/4)] + \frac{3\tilde{\lambda}(4+\tilde{\lambda}^2)}{1024(4+\tilde{\lambda})}\mathrm{dilog}\left(\frac{4+\tilde{\lambda}H}{4+\tilde{\lambda}}\right) \\ & - \left\{\frac{3\tilde{\lambda}^3[7\tilde{\lambda}+256\,Y(\tilde{\lambda})]}{32768(4+\tilde{\lambda})} + \frac{3\tilde{\lambda}(4+\tilde{\lambda}H)}{32768H^2}[H(7\tilde{\lambda}+8)+4]\right\}\log(4+\tilde{\lambda}H) \\ & + \left\{\left[\frac{3\tilde{\lambda}(\tilde{\lambda}-4)-16}{128}\right]Y(\tilde{\lambda}) + \frac{3\tilde{\lambda}[1+2(1+\tilde{\lambda})H]+4H^2}{2048H^2}\right\}\log(H) \\ & - \left\{\frac{3\tilde{\lambda}[16+7\tilde{\lambda}(4-\tilde{\lambda})]}{32768}\right\}\log(H) + \frac{1+\tilde{\lambda}}{2(4+\tilde{\lambda})}\left[Y(\tilde{\lambda}) + \frac{3\tilde{\lambda}-2}{128}\right]\log(H-1) \\ & + \left[\frac{2+H(4+3\tilde{\lambda})}{32H^2}\right]Y(\tilde{\lambda}) - \frac{3\tilde{\lambda}(1+\tilde{\lambda})}{512}(\log 2)^2 - \frac{\pi^2\tilde{\lambda}(1+\tilde{\lambda})}{2048} \\ & + \frac{9\tilde{\lambda}}{65536}\log(\tilde{\lambda})\log(4+\tilde{\lambda}H) + \frac{3\tilde{\lambda}^2}{65536}[2(8+7\tilde{\lambda}) - 3\tilde{\lambda}^2\log(\tilde{\lambda})]\log(\tilde{\lambda}H) \\ & - \frac{3\tilde{\lambda}(1+\tilde{\lambda})}{2048}\left[(\log(H))^2 - 4\log 2\log(\tilde{\lambda}H) - \log(4+\tilde{\lambda})\log\left(\frac{4+\tilde{\lambda}}{(H-1)^2}\right)\right] \\ & + \frac{1}{8192H^3}\left[(42\tilde{\lambda}^2+36\tilde{\lambda}-16)H^2 + 4(3\tilde{\lambda}-2)H - \frac{16}{3}\right], \end{aligned} \tag{C 2}$$

where it is recalled that $H = 1 + s^2$ and the new quantity $Y(\tilde{\lambda})$ is defined as $Y(\tilde{\lambda}) = [2 - 3\tilde{\lambda} + +3\tilde{\lambda}(4+\tilde{\lambda})\log(4+\tilde{\lambda})/4]/128$.

REFERENCES

Abramowitz, M. & Stegun, I. A. 1965 *Handbook of Mathematical Functions*. Dover Publications.

Bazant, M. & Vinagradova, O. I. 2008 Tensorial hydrodynamic slip. *J. Fluid Mech.* **613**, 125–134.

Beavers, G. & Joseph, D. 1967 Boundary conditions at a naturally permeable wall. *J. Fluid Mech.* **30**, 197–207.

Brinkman, H. 1947 A calculation of the viscous force exerted by a flowing fluid on a dense swarm of particles. *Appl. Sci. Res.* A **1**, 27–34.

Carotenuto, C. & Minale, M. 2011 Shear flow over a porous layer: velocity in the real proximity of the interface via rheological tests. *Phys. Fluids* **23** (6), 063101.

Darcy, H. 1856 *Les Fontaines Publiques de la Ville de Dijon*. Dalmont.

Davis, A. M. J., Kezirian, M. T. & Brenner, H. 1994 On the Stokes–Einstein model of surface diffusion along solid surfaces: slip boundary conditions. *J. Colloid Interface Sci.* **1065**, 129–140.

DEBBECH, A., ELASMI, L. & FEUILLEBOIS, F. 2010 The method of fundamental solution for the creeping flow around a sphere close to a membrane. *Z. Angew. Math. Mech.* **90** (12), 920–928.

ELASMI, L. & FEUILLEBOIS, F. 2001 Green function for a Stokes flow near a porous slab. *Z. Angew. Math. Mech.* **81** (11), 743–752.

ELASMI, L. & FEUILLEBOIS, F. 2003 Integral equation method for creeping flow around a solid body near a porous slab. *Q. J. Mech. Appl. Math.* **56** (2), 163–185.

GHALIA, N., FEUILLEBOIS, F. & SELLIER, A. 2016 A sphere in a second degree polynomial creeping flow parallel to a plane, impermeable and slipping wall. *Q. J. Mech. Appl. Maths* **69**, 353–390.

GOREN, S. L. 1973 The hydrodynamic force resisting the approach of a sphere to a plane wall in slip flow. *J. Colloid Interface Sci.* **44** (2), 356–360.

GOREN, S. L. 1979 The hydrodynamic force resisting the approach of a sphere to a plane permeable wall. *J. Colloid Interface Sci.* **69** (1), 78–85.

HANDY, W. B. & BIRCUMSHAW, I. 1925 Bakerian lecture. Boundary lubrication – plane surfaces and the limitations of Amontons' law. *Proc. R. Soc. Lond.* A **108** (745), 1–27.

HOCKING, L. M. 1973 The effect of slip on the motion of a sphere close to a wall and of two adjacent spheres. *J. Engng Maths* **7** (3), 207–221.

KARMAKAR, T. & RAJA SEKHAR, G. P. 2018 Squeeze-film flow between a flat impermeable bearing and an anisotropic porous bed. *Phys. Fluids* **30**, 043604.

LE-CLECH, P., CHEN, V. & FANE, T. A. G. 2006 Fouling in membrane bioreactors used in wastewater treatment. *J. Membr. Sci.* **284**, 17–53.

LECOQ, N., ANTHORE, R., CICHOCKI, B., SZYMCZAK, P. & FEUILLEBOIS, F. 2004 Drag force on a sphere moving towards a corrugated wall. *J. Fluid Mech.* **513**, 247–264.

LIN, J.-R., LU, R.-F. & YANG, C.-B. 2001 Derivation of porous squeeze-film Reynolds equations using the Brinkman model and its application. *J. Phys.* D *Appl. Phys.* **34**, 3217–3223.

LOUSSAIEF, H., PASOL, L. & FEUILLEBOIS, F. 2015 Motion of a spherical particle in a viscous fluid along a slip wall. *Q. J. Mech. Appl. Maths* **68** (2), 115–144.

LUO, H. & POZRIKIDIS, C. 2008 Effect of surface slip on Stokes flow past a spherical particle in infinite fluid and near a plane wall. *J. Engng Maths* **62**, 1–21.

MICHALOPOULOU, A. C., BURGANOS, V. N. & PAYATAKES, A. C. 1992 Creeping axisymmetric flow around a solid particle near a permeable obstacle. *AIChE J.* **38** (8), 1213–1228.

NAVIER, C. L. M. H. 1823 Mémoire sur les lois du mouvement des fluides. *Mémoires de l'Acad. des Sciences de l'Institut de France* **6**, 389–416.

NGUYEN, A. V. 2000 Historical note on the Stefan–Reynolds equations. *J. Colloid Interface Sci.* **231** (1), 195.

NIELD, D. A. & BEJAN, A. 2006 *Convection in Porous Media*. Springer.

NIR, A. 1981 On the departure of a sphere from contact with a permeable membrane. *J. Engng Maths* **15** (1), 65–75.

OCHOA-TAPIA, J. A. & WHITAKER, S. 1995*a* Momentum transfer at the boundary between a porous medium and a homogeneous fluid. I. Theoretical development. *Intl J. Heat Mass Transfer* **38** (14), 2635–2646.

OCHOA-TAPIA, J. A. & WHITAKER, S. 1995*b* Momentum transfer at the boundary between a porous medium and a homogeneous fluid. II. Comparison with experiment. *Intl J. Heat Mass Transfer* **38** (14), 2647–2655.

RAMON, G. Z., HUPPERT, H. E., LISTER, J. R. & STONE, H. A. 2013 On the hydrodynamic interaction between a particle and a permeable surface. *Phys. Fluids.* **25**, 073103.

REYNOLDS, O. 1886 IV. On the theory of lubrication and its application to Mr. Beauchamp Tower's experiments, including an experimental determination of the viscosity of olive oil. *Phil. Trans. R. Soc. Lond.* **177**, 157–234.

SAFFMAN, P. G. 1971 On the boundary condition at the surface of a porous medium. *Stud. Appl. Maths* **1** (2), 93–101.

SHERWOOD, J. D. 1988 The force on a sphere pulled away from a permeable half-space. *Physico-Chem. Hydrodyn.* **10** (1), 3–12.

VINOGRADOVA, O. I. 1995 Drainage of a thin liquid film confined between hydrophobic surfaces. *Langmuir* **11**, 2213–2220.

WU, Z. & MIRBOD, P. 2018 Experimental analysis of the flow near the boundary of random porous media. *Phys. Fluids* **30** (4), 047103.